Photosynthetic water oxidation at elevated dioxygen partial pressure monitored by time-resolved X-ray absorption measurements

Michael Haumann[1], Alexander Grundmeier, Ivelina Zaharieva, and Holger Dau[1]

Freie Universität Berlin, Institut für Experimentalphysik, Arnimallee 14, 14195 Berlin, Germany

Edited by Harry B. Gray, California Institute of Technology, Pasadena, CA, and approved September 26, 2008 (received for review March 19, 2008)

The atmospheric dioxygen (O_2) is produced at a tetramanganese complex bound to the proteins of photosystem II (PSII). To investigate product inhibition at elevated oxygen partial pressure (pO_2 ranging from 0.2 to 16 bar), we monitored specifically the redox reactions of the Mn complex in its catalytic S-state cycle by rapid-scan and time-resolved X-ray absorption near-edge spectroscopy (XANES) at the Mn K-edge. By using a pressure cell for X-ray measurements after laser-flash excitation of PSII particles, we found a clear pO_2 influence on the redox reactions of the Mn complex, with a similar half-effect pressure as determined (2–3 bar). However, XANES spectra and the time courses of the X-ray fluorescence collected with microsecond resolution suggested that the O_2 evolution transition itself ($S_3 \Rightarrow S_0 + O_2$) was not affected. Additional (nonstandard) oxidation of the Mn complex at high pO_2 explains our experimental findings more readily. Our results suggest that photosynthesis at ambient conditions is not limited by product inhibition of the O_2 formation step.

manganese complex | photosystem II | X-ray spectroscopy | bioinorganic chemistry | oxygen pressure

In oxygenic photosynthesis, plants, algae, and cyanobacteria facilitate the primary biomass formation by exploiting solar energy for driving the conversion of water (H_2O) and carbon dioxide (CO_2) into carbohydrates ($C_nH_{2n}O_n$). Dioxygen (O_2) is formed as product of the water oxidation chemistry of the photosystem II (PSII) protein complex (1–5). Photosynthetic CO_2 fixation and O_2 formation have shaped the Earth's atmosphere (6) by (*i*) lowering the CO_2 level to $<0.04\%$ and (*ii*) creation of a maximal O_2 concentration of 35% (7), ≈300 million years before the present and a current level of ≈20%.

In photosynthetic organisms, the low level of atmospheric CO_2 can limit photosynthesis, related to the activity of CO_2-fixing ribulose bisphosphate carboxylase (8, 9). It is less clear whether water oxidation by PSII is directly affected by the concentration of O_2, the immediate product of light-driven water splitting. This question was only recently addressed experimentally by Clausen and Junge (10). They exposed PSII from cyanobacteria to oxygen partial pressures (pO_2) ranging from 0.2 to 30 bar and, analyzing flash-induced near-UV absorption changes, discovered a pO_2 effect with a half-saturation pressure of only ≈2 bar (10). Subsequently, in measurements of delayed Chl fluorescence, together with Clausen and Junge we confirmed that also the donor side of the plant PSII in its native membrane environment is affected by elevated pO_2 (11). The surprisingly low half-pressure of only 2–3 bar was taken as an indication that the efficiency of the O_2 formation step could be reduced significantly by product inhibition. Such a limitation of the water oxidation chemistry may have imposed restraints on the evolution of oxygenic photosynthesis (10). Notably, the pO_2 inside of photosynthetic cells in microbial mats and bioreactors can be severalfold higher than the atmospheric level of 0.2 bar (12). Thus, inhibition of O_2 formation already at moderate pO_2 could limit photosynthetic productivity in present ecosystems and future biotechnological applications.

The catalyst of photosynthetic water oxidation is a Mn_4Ca complex bound to PSII (1–5). Tentative atomic models of the complex resulted from crystallographic and X-ray absorption data (13, 14). Frequently, the Mn complex, its ligand environment, and a nearby redox-active tyrosine residue [Y_Z, Tyr-160/161 of the D1 protein (15)] are denoted as oxygen-evolving complex (OEC). The paradigmatic functional model for discussion of the redox reactions of the OEC has been proposed already in 1970 by Kok *et al*. (15), accounting for the period-of-four pattern in the flash-number dependence of O_2 formation first observed by Joliot and Joliot (16). The Kok cycle involves the states S_0–S_4; the subscript indicates the number of oxidizing equivalents accumulated by the OEC (15, 17). The OEC can be driven synchronously through the S-state cycle by the application of saturating flashes of visible light. After dark adaptation, the S_1-state prevails, and each light flash induces a specific transition: 1st flash, $S_1 \rightarrow S_2$; 2nd flash, $S_2 \rightarrow S_3$; 3rd flash, $S_3 \rightarrow S_4 \rightarrow S_0 + O_2$; 4th flash, $S_0 \rightarrow S_1$. Increasing desynchronization of the S-state population is the result of so-called miss events caused by competition between forward electron transfer and charge recombination processes (18–21).

The chemistry of photosynthetic water oxidation still is not completely understood (1, 5). Four semistable intermediate states of the reaction cycle (S_0, S_1, S_2, S_3) are well characterized. Identification of further, transiently formed reaction intermediates may pave the road toward a more complete understanding of the reaction mechanism. Recently, we have shown that formation of the S_4-state involves a reaction intermediate that likely is formed by a deprotonation step (22, 23). These and other findings facilitated an extension of the classical S-state cycle model (17, 24). On the basis of their O_2 pressure experiments, Clausen and Junge have proposed that in the $S_4 \rightarrow S_0$ transition a reaction intermediate is formed where water is partially oxidized to the peroxide level, and the Mn complex concomitantly is reduced to a level equivalent to the S_2-state (S_2^*, see Fig. 1). The proposed S_2^*-state differs from the intermediate described in ref. 22, as clarified elsewhere (24–26).

The mechanistic importance of a peroxidic reaction intermediate prompted us to investigate the influence of an elevated pO_2 on the redox reactions by rapid-scan and time-resolved X-ray absorption spectroscopy (XAS) at the Mn K-edge (22, 27–29), where the spectral changes exclusively reflect structure and oxidation state changes of the Mn complex of PSII (30–32).

Author contributions: M.H. designed research; M.H., A.G., and I.Z. performed research; M.H. and H.D. analyzed data; and M.H. and H.D. wrote the paper.

The authors declare no conflict of interest.

This article is a PNAS Direct Submission.

[1]To whom correspondence may be addressed. E-mail: haumann@physik.fu-berlin.de or holger.dau@physik.fu-berlin.de.

This article contains supporting information online at www.pnas.org/cgi/content/full/0802596105/DCSupplemental.

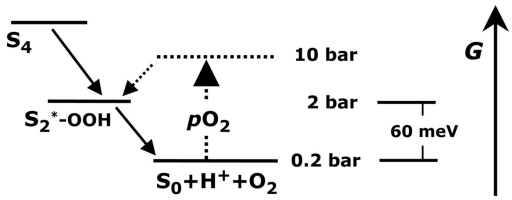

Fig. 1. Hypothetical energy-level diagram for a thermodynamic O_2 back-pressure effect on the $S_4 \rightarrow S_0$ transition. The Gibbs free energy, G_P, of the final product state ($S_0 + O_2$) increases by ≈60 meV per 10-fold pO_2 increase. At $pO_2 > 10$ bar, the energy of a peroxidic reaction intermediate was predicted to be higher than G_P, implying almost complete inhibition of O_2 formation (10). The energy of the S_2* reaction intermediate has been proposed to be above (10) or below (11) the initial $Y_2^{ox}S_3$-state. In the present work, validity of the above scheme is scrutinized and eventually rejected.

Results

X-Ray Photoreduction at Elevated pO_2. For X-ray absorption measurements (at 20 ± 1 °C), the PSII samples were placed in a cell sustaining O_2 pressures up to 20 bar [supporting information (SI) *Materials and Methods* and Fig. S1], and the S-state transitions of the Mn complex were induced by nanosecond laser flashes. Modification of the oxidation state of the Mn complex by X-ray irradiation (33–35) was studied at various pO_2 levels. No specific O_2 effect on X-ray photoreduction was found (*SI Materials and Methods* and Fig. S2). For all of the following experiments, the X-ray intensities were adjusted such that the Mn oxidation state remained unchanged during measurements (negligible Mn photoreduction).

X-Ray Absorption Near-Edge Structure (XANES) Spectra at Atmospheric and Elevated pO_2. XANES spectra were recorded immediately after excitation of PSII samples in the pressure cell by 0–6 laser flashes (Fig. 2 *A* and *B*). At ambient pO_2 (0.2 bar), similar shifts of the K-edge to higher energies on flashes 1 and 2 were detected as previously (32, 36). They are attributable to oxidation of the Mn complex in the $S_1 \rightarrow S_2$ and $S_2 \rightarrow S_3$ transitions. After the 3rd flash, the edge shifted to lower energies because of Mn reduction by electrons from water in the O_2 evolution step ($S_3 \rightarrow S_4 \rightarrow S_0$) (Fig. 2*A*). The corresponding edge energies are depicted in Fig. 3*A* (filled circles). At a pO_2 of 11 bar, shifts of the K-edge energy also were observed (Fig. 2*B*), but at increasing flash numbers their magnitudes differed from those at ambient pO_2, suggesting that the redox chemistry of the Mn complex was altered by an elevated pO_2 (Figs. 2*B* and 3*B*).

Time-Resolved X-Ray Experiments at elevated pO_2. The changes in the XANES spectra in Fig. 2 merely reflect the net effect of Mn oxidation and reduction because by illumination with a sequence of Laser flashes, the Mn complex is not driven fully synchronously through its reaction cycle. Among other things, because of incomplete turnover of PSII (miss events), "S-state scrambling" occurs on higher flash numbers. For example, the 3rd flash induces not only Mn reduction and O_2 formation ($S_3 \rightarrow S_4 \rightarrow S_0$), but also Mn oxidation in a sizable fraction of the PSII population (mostly $S_2 \rightarrow S_3$ transition). Time-resolved X-ray absorption measurements on dark-adapted PSII samples facilitate disentangling of the oxidation and reduction processes.

For a sequence of 10 laser flashes, time courses of the X-ray fluorescence ($F_{X\text{-ray}}$) at constant X-ray excitation energy (6,552.5 eV) were recorded (Fig. 4) (22, 29). A decrease in the fluorescence level after the flash indicates oxidation of the Mn complex, an increase reflects Mn reduction. [We note that the magnitude of $\Delta F_{X\text{-ray}}$ is S-state-dependent; for excitation at 6,552.5 eV, it is larger in $S_1 \rightarrow S_2$ than in $S_2 \rightarrow S_3$ (36–38).] At 0.2 bar O_2, Mn reduction was absent on flash 1 and small on flash 2, whereas at

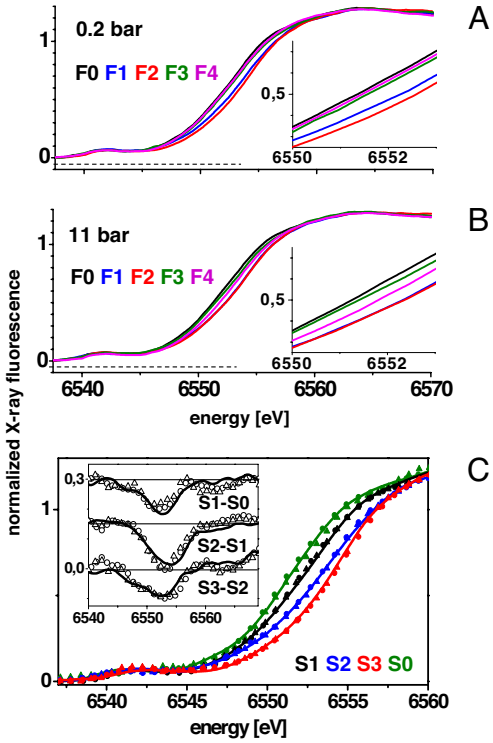

Fig. 2. XANES spectra of the Mn complex measured after the application of 0–4 laser flashes to PSII samples at pO_2 of 0.2 bar (*A*) and 11 bar (*B*). Spectra are the average of 2 (0.2 bar) and 4 (11 bar) sets of independently measured spectra. (*Insets*) Expanded half-height region of the K-edges. (*C*) Calculated spectra of pure S-states (color code as indicated), obtained by deconvolution of the spectra in *A* and *B* using parameters listed in Table 1 [lines, 0.2 bar; triangles, 11 bar O_2 (a); dots, 11 bar O_2 (b)] and in the legend of Fig. 3. (*Inset*) Corresponding difference spectra.

13 bar O_2, significant Mn reduction occurred already on flash 2. The average fluorescence level at flash numbers >3 was lower than that at 0.2 bar, suggesting a higher mean K-edge energy, in agreement with the XANES spectra. Furthermore, the K-edge shifts estimated on basis of the X-ray transients in Fig. 4 and from the XANES spectra compare well (Fig. 3, open triangles and filled circles).

It has been suggested that at elevated pO_2, the 3rd flash does not induce a 4-electron reduction of the Mn complex, but a 2-electron reduction resulting in a peroxidic intermediate (S_2*) (10, 11). According to this rationale, a diminished amplitude of the Mn reduction transient on flash 3 may be expected at high pO_2. However, as clearly visible in Fig. 4 *Right*, flash 3, the magnitude of the Mn reduction (millisecond increase marked by a filled arrow) was not diminished at 13 bar O_2, suggesting that rather than a 2-electron reduction, the usual 4-electron reduction of Mn was induced by the 3rd flash. Furthermore, the X-ray transients show that on higher flash numbers also at 13 bar O_2, each flash induces Mn oxidation and reduction; the average magnitude of the flash-induced transients is not smaller than at 0.2 bar (Fig. 5*B*). Thus, inhibition of the light-triggered redox reactions by accumulation of an S_2* intermediate can be excluded. We feel that the X-ray transients of Fig. 4 cannot be reconciled in a reasonably straightforward way with the proposed S_2* formation in a major fraction of PSII (10, 11).

What causes the differences between the X-ray data collected at atmospheric and elevated O_2 pressures? The time-resolved data indicates, for elevated pO_2, significant Mn reduction and hence O_2 formation already on the 2nd flash (Fig. 4). Simula-

BIOPHYSICS

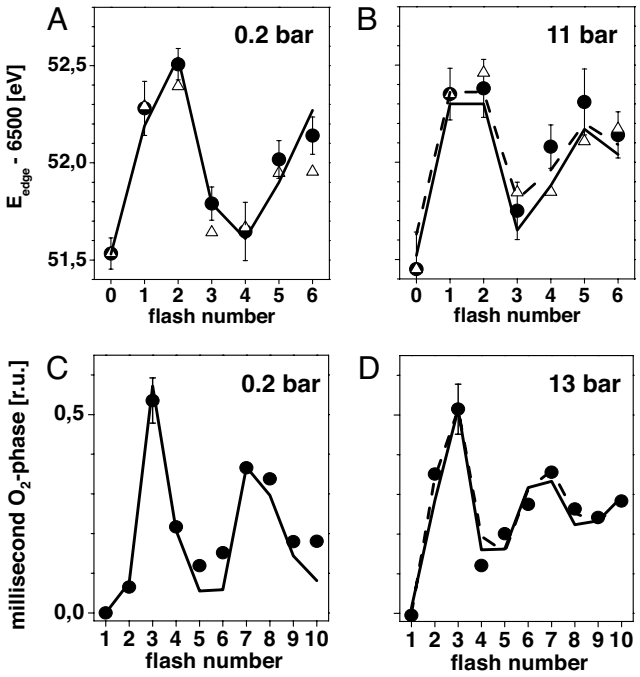

Fig. 3. Mn K-edge energies (filled circles) determined from spectra as in Fig. 2 (*A*, 0.2 bar; *B*, 11 bar O_2). Error bars represent SD values from 2 (at 0.2 bar) and 4 (at 11 bar) datasets. The lines were obtained by simulation of the flash patterns using the parameters listed in Table 1 [in *B*: solid line (a), dashed line (b)]. An S_1-state edge energy of 6,551.5 eV and edge shifts as determined in (27, 28) were used in the simulations. (*C* and *D*) Filled circles represent the magnitude of the millisecond rise in the X-ray absorption at 6,552.5 eV (Fig. 4) caused by Mn reduction in the $S_3 \rightarrow S_4 \rightarrow S_0$ transition. Edge energy estimates derived from the X-ray transients in Fig. 4 are shown for comparison in *A* and *B* (open triangles, assuming direct proportionality between edge shift and X-ray fluorescence change for excitation at 6,552.5 eV; normalization to equal first-flash response). Lines in *C* and *D* show simulations with parameters in Table 1 [in *D*: (a) solid line, (b) dashed line].

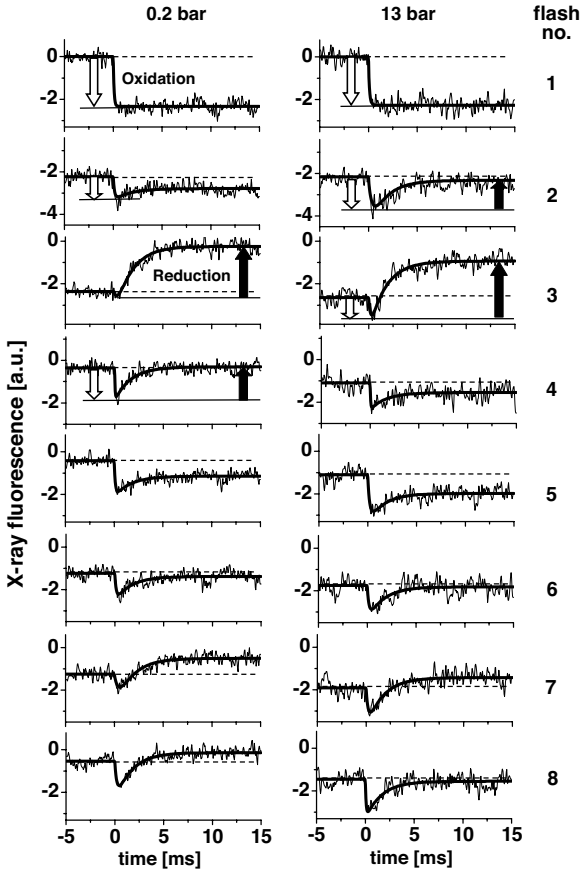

Fig. 4. Time courses of the X-ray fluorescence at pO_2 of 0.2 bar (*Left*) and 13 bar (*Right*) as induced by the first 8 of a train of 10 laser flashes applied to dark-adapted PSII samples (excitation energy of 6,552.5 eV). Approximately 500 (0.2 bar) and 1,500 (13 bar) transients were averaged and are displayed at a resolution of 50 μs per data point. The 13 bar transients were obtained by averaging measurements for pO_2 values ranging from 11 to 16 bar. Data were normalized such that the amplitude of the response to the 1st flash was similar for the 0.2 and the 13 bar datasets. Smooth lines represent simulations by a biexponential function using a halftime of 1.2 ms to account for Mn reduction (positively directed changes) and variable halftimes for Mn oxidation (negatively directed signals). For selected transients the contributions from Mn oxidation (open arrows) and Mn reduction (filled arrows) are indicated.

tions on the basis of Kok's S-state model (15, 36) of the data in Fig. 4 were used to characterize and quantify the O_2 effects.

Simulations of the Flash Number Dependence in the X-Ray Data. Curve fitting of the X-ray transients in Fig. 4 (smooth lines) yielded the amplitudes caused by Mn reduction ($t_{1/2} \approx 1.2$ ms). The quaternary oscillations of (*i*) the millisecond amplitude (Fig. 3 *C* and *D*), (*ii*) the *K*-edge energy (Fig. 3 *A* and *B*), and the complete XANES spectra (Fig. 2*C*) can be described by similar sets of transition parameters for all 0.2-bar data, on the one hand, and similar parameter sets for all high-pO_2 data (Table 1). The parameters for the 0.2-bar data are close to determined values (36). Two simulation approaches with alternative parameter sets described the high-pO_2 data similarly well (Table 1).

"Apparent" double-hits on all S-state transitions (Fig. 3* B *and* D*; solid lines). The classical double-hits (15) were excluded because of the use of nanosecond laser flashes. An option to rationalize an apparent double-hit at high pO_2 is rapid formation of reactive oxygen species (ROS) (39–41) that then oxidize the Mn complex. The comparably large magnitude of Mn reduction in the time-resolved X-ray data (Fig. 4; sum of reduction phases on the first 4 flashes) and the large edge-shift on flash 1 ($S_1 \rightarrow S_2$) in the *K*-edge spectra (Fig. 2) are in agreement with surplus flash-induced Mn oxidation.

Increased initial S_2 population in the samples plus a large apparent double-hit probability in the $S_0 \rightarrow S_1$ transition only (Fig. 3* B *and* D*; dashed lines). This simulation approach could correspond to slow dark oxidation of the S_1-state (before flash 1) and more rapid dark oxidation of the S_0-state (between flashes 3 and 4). To assess S_2 formation by dark oxidation of the S_1-state (at high pO_2), we used EPR spectroscopy. In dark-adapted PSII samples that had been exposed to 15 bar O_2 for 30 min, the typical EPR multiline signal of the S_2-state (42) was not detectable (Fig. S3). Thus, dark oxidation resulting in formation of the normal S_2-state can be excluded (but not the generation of an EPR-silent modified S_2-state).

Assuming the absence of any specific influence of elevated pO_2 on the $S_3 \rightarrow S_4 \rightarrow S_0$ transition and by using the altered parameters discussed above, the XANES spectra of the pure S-states were calculated. The resulting high-pO_2 spectra, within the precision of the experiment, are identical to the low-pO_2 spectra of the pure S-states (Fig. 2*C*). Accordingly, the XANES spectra at high pO_2 can be explained without invoking any S_2^* formation.

We emphasize that all simulations involving S_2^* formation in a sizeable fraction of PSII ($\geq$10%), followed either by an $S_2^* \rightarrow S_2$ or $S_2^* \rightarrow S_0$ transition in the dark or a blockage in the S_2^*-state, consistently failed to describe the experimental results

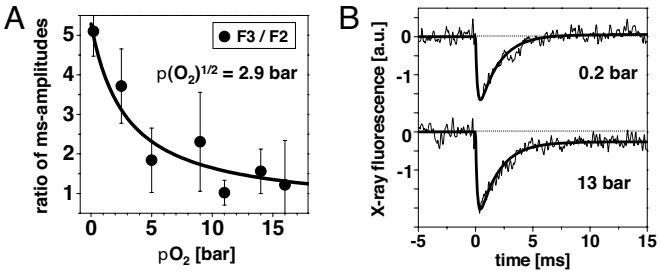

Fig. 5. Half-effect O_2 pressure and rate of Mn reduction. (*A*) Pressure dependence of the O_2 effect on PSII and (*B*) averaged X-ray transients collected at 0.2 and 13 bar. (*A*) Amplitudes of the millisecond phases were determined for the X-ray transients induced by the 2nd and 3rd flashes; the ratio of these amplitudes is shown (filled circles; error bars denote SD). The line represents an asymptotic simulation with a $pO_2^{1/2}$ of 2.9 bar. (*B*) Transients represent the average of the transients on the first 10 flashes applied to dark-adapted PSII. Smooth lines denote biexponential simulations. The signal rise associated with Mn reduction in the $S_3 \rightarrow S_4 \rightarrow S_0$ transition was simulated with an identical halftime of 1.2 ms for transients collected at pO_2 of 0.2 and 13 bar. The initial decrease was approximated by an exponential function with halftimes of Mn oxidation of 105 ± 20 μs (0.2 bar) and 120 ± 20 μs (13 bar).

(data not shown). The above simulations support the conclusion already drawn from visual inspection of the X-ray transients of Fig. 4, namely the absence of a high-pO_2 influence on the $S_3 \rightarrow S_4 \rightarrow S_0$ transition itself. The high-pO_2 effect detected here is explainable by additional oxidations of the Mn complex that are either light-induced (1st simulation approach) or proceed in the dark (2nd approach).

O_2 Half-Saturation Pressure. Time-resolved experiments were performed at pO_2 values ranging from 0.2 to 16 bar (time courses not shown), and the millisecond amplitudes of Mn reduction were determined for each flash. Then, the ratio of millisecond amplitudes on flashes 2 and 3 was calculated (F3/F2; Fig. 5*A*) as a relative measure of the alterations in the S-state distribution. The pronounced decrease in F3/F2 with increasing pO_2 was described by a $pO_2^{1/2}$ of 2.9 bar (Fig. 5*A*, line); saturation occurred at ≈10 bar. Thus, the pO_2 of ≥10 bar in the XAS measurements discussed above was sufficient to saturate the O_2 effects. A similar $pO_2^{1/2}$ value has been observed in previous O_2 experiments on different types of PSII samples (10, 11).

Halftimes of Mn Oxidation and Reduction. The halftimes of Mn oxidation and reduction were determined from the time-resolved X-ray data (Fig. 5*B*). To improve the signal-to-noise ratio, the transients of the first 10 flashes (for flashes 1–8, see Fig. 4) were averaged and subjected to a biexponential simulation (lines). The amplitude of the oxidation–reduction transient is slightly increased at high pO_2, possibly explainable by additional, nonstandard oxidations of the Mn complex shortly after flash excitation (model a in Table 1). By using at 13 bar and 0.2 bar an identical halftime of Mn reduction of 1.2 ± 0.1 ms, a value that is typical for PSII (10, 11), convincing simulations were obtained. Furthermore, an apparent mean halftime of Mn oxidation of ≈110 μs (Fig. 5*B*, see legend) was derived, which also was identical at 0.2 and 13 bar pO_2 (within the error range). In conclusion, the X-ray transients suggest unchanged halftimes of Mn reduction in the O_2 formation step and of Mn oxidation at high pO_2.

Discussion

Already at moderately elevated pO_2 (half-effect pressure of 2–3 bar), the redox chemistry of the PSII manganese complex is modified, as found in refs. 10 and 11. However, the X-ray absorption data do not indicate inhibition of the oxygen evolution transition (i.e., $S_3 \rightarrow S_4 \rightarrow S_0 + O_2$). Specifically, the formation of a partially reduced state of the Mn complex resembling the S_2-state (S_2^*) in a major fraction of PSII (5) cannot be reconciled with the experimental findings of the present investigation. In conclusion, the thermodynamic product inhibition illustrated in Fig. 1 is not observed.

The high-pO_2 effects in the X-ray data can be rationalized by Mn oxidation by ROS formed upon flash illumination (39–41, 43) and/or dark oxidation of the S_0 and S_1-state, the 2 low-potential S-states (5). Either option is sufficient to model adequately the X-ray data. For additional flash-induced oxidations, a plausible mechanistic scenario is that oversaturating laser flashes at high pO_2 result in especially pronounced chlorophyll triplet (^{3}Chl) and singlet oxygen ($^1O_2$) formation (39, 43). The high-oxidation potential of $^1O_2$, its extreme reactivity, and a diffusion length on the order of 100 Å could facilitate direct or indirect oxidation of the Mn complex, possibly resulting in superoxide formation (39–41).

The O_2/H_2O midpoint potential (E_m) at elevated pO_2 (≈0.95 V at 10 bar and pH 6.2) is close to the estimated E_m of the Mn complex in its S_1- and S_0-states, but likely too low for dark oxidation of the S_2- and S_3-states (5). Thus, dark oxidation of the lower S-states may be thermodynamically feasible at high pO_2; it could be indirect, involving other cofactors and/or ROS. Our finding that high-pO_2 exposure does not result in formation of the typical S_2-state EPR signal disfavors dark oxidation of S_1 to a normal S_2-state. However, formation of a modified S_2-state cannot be excluded. Further studies are required to clarify the mode of O_2 interaction with the Mn complex.

Clausen and Junge (10) have discovered the pO_2 influence on the redox reactions of the PSII Mn complex by means of analysis of flash-induced UV absorption changes. Subsequently we investigated, in cooperation with Clausen and Junge, the pO_2 effect by time-resolved measurements of delayed chlorophyll fluorescence (DF) (11). In both studies it was suggested that at saturating pO_2 (>10 bar), dioxygen formation is blocked because of formation of a peroxidic S_2^* intermediate (10). Our present results rather exclude S_2^* formation in a sizeable fraction of PSII. The 2 spectroscopic methods used in refs. 10 and 11 do not reflect specifically the oxidation state changes of the Mn com-

Table 1. Simulation parameters (in percentage)

	pO_2, bar	Initial S_0, S_1, S_2, S_3	Miss factor	Double hits	Non-Q_B centers
XANES spectra	0.2	10, 80, **10**, 0	15	**0**	15
	11(a)	10, 80, **10**, 0	7	**14**	15
	11(b)	10, 60, **30**, 0	15	**55**	15
X-ray time scans	0.2	0, 90, **10**, 0	12	**0**	10
	13(a)	0, 90, **10**, 0	9	**14**	10
	13(b)	0, 60, **40**, 0	12	**35**	10

The simulation results are shown as lines in Fig. 3. Values revealing pronounced changes at elevated pO_2 are marked bold. (a) Uniform double hit probability on all four S-transitions. (b) Apparent double hits only on the $S_0 \rightarrow S_1$ transition.

plex. The resulting ambiguity in combination with a modeling approach that did not include the possibility of additional, nonstandard oxidations may explain the diverging conclusions on the pO_2 effect in refs. 10 and 11.

Differences in the results of the present and previous studies also could originate from unequal experimental conditions. Specifically, the reactions of ROS with PSII may have been different in the current and previous investigations. They could depend on experimental details such as sample thickness (here only ≈300 μm, thus possibly particularly rapid pO_2 equilibration) and PSII concentration (here much higher than in the solution studies). Whether the thermodynamics of the water oxidation cycle of the intact Mn complex itself depends critically on these experimental details is still unclear but, in our opinion, unlikely.

Even at a pO_2 >10 bar, we have not obtained any indication for O_2 product inhibition of the $S_3 \rightarrow S_4 \rightarrow S_0$ transition itself. An increase in pO_2 from 0.2 to 10 bar corresponds to an increase in G_P, the Gibbs free energy of the product state ($Y_Z{}^0S_0+O_2$), by

$$\Delta G_P \approx 60 \text{ meV} \cdot \log(10 \text{ bar}/0.2 \text{ bar}) \approx 100 \text{ meV}. \quad [1]$$

We conservatively estimate that any inhibition of the $S_3 \rightarrow S_0$ transition that affected >30% of the PSII would have been resolvable. This implies that also at pO_2 >10 bar, the free-energy level, G_I, of an intermediate in the $S_3 \rightarrow S_4 \rightarrow S_0$ transition lies above G_P by a value that corresponds to an equilibrium constant of ≈3. Thus, we obtain for ΔG_{I-P} ($= G_I - G_P$):

$$\Delta G_{I-P} > 100 \text{ meV} + 60 \text{ meV} \log(3) \approx 130 \text{ meV}. \quad [2]$$

In conclusion, we estimate that the free energy of the product state ($Y_Z{}^0S_0+O_2$ at pH 6.2) is ≥130 meV below the free-energy level of any intermediate in the $S_3 \rightarrow S_4 \rightarrow S_0$ transition.

The basic reaction cycle of the Mn complex discussed elsewhere (17, 24) implies that O_2 formation in the $S_4 \rightarrow S_0$ transition is associated with the release of 1 proton. Consequently, the free energy of the product state is predicted to rise upon acidification by ≈60 meV per pH unit. In intact organisms, the pH in the thylakoid lumen drops upon illumination to values between 5 and 6 (44). At pH 5, G_P thus may be by ≈70 meV higher than at pH 6.2, resulting in a decrease of the minimal ΔG_{I-P} to ≈60 meV. This figure implies that at atmospheric pO_2 even in the presence of a luminal acidification, a sizable O_2 product inhibition is unlikely.

Our results suggest that the rate of photosynthetic water oxidation is not seriously limited by thermodynamic product inhibition of the O_2 evolution transition. Growth limitations at elevated pO_2 may root in diverse oxidative processes (40) but presumably not in inhibition of the O_2 formation step. It remains an open question whether the insensitivity of the O_2 formation step to product inhibition reported here has always been a feature of PSII or has evolved concomitantly with the increase in the atmospheric pO_2.

Materials and Methods

XAS samples of high-activity PSII membrane particles from spinach (45) were prepared by pipetting PSII suspensions (10 μL, ≈12 mg of Chl mL^{-1}, containing 100 μM phenyl-p-benzoquinone (PPBQ) as an electron acceptor) into each of the 20 cavities of the sample holders (29) to be inserted into the pressure cell. Samples were partially dehydrated (loss of ≈20% of the initial water content) by drying in a desiccator for 1 h over silica gel at 0.5 bar of air pressure at 4 °C and then frozen in liquid nitrogen. Compared with previous studies (22, 36), this procedure resulted in a higher water content of the samples ensuring (*i*) that prolonged exposure to an atmosphere of dry O_2 gas did not cause any dehydration detrimental to sample integrity and (*ii*) an almost isotropic orientation of the PSII membrane particles so that magic-angle excitation was not required and XAS could be performed at an excitation angle of 45°. To maximize the S_1-state content, each sample was illuminated by a single saturating flash and then dark-adapted for 1 h during the drying period. Approximately 300 stripes with 20 sample cavities each were prepared (≈6,000 PSII samples in total).

X-ray experiments at the Mn K-edge were carried out at the undulator beamline ID26 at the European Synchrotron Radiation Facility at Grenoble, France, employing developed techniques for time-resolved XAS measurements (22, 29). The 3 undulators of the beamline were adjusted such that an approximately flat intensity profile of the exciting X-ray beam resulted in the region of the Mn K-edge (maximal X-ray flux ≈10^{13} photons s^{-1}, spot size 1 × 1.5 mm^2, attenuated by stacked Al foils whenever required). A newly constructed pressure cell sustaining O_2 pressures up to 20 bar was used (see *SI Materials and Methods*). For measurements at elevated pO_2, (1) the cell was flushed (cap slightly unscrewed) for 10 s with O_2 gas of highest purity (2). The cap of the cell was closed, and the pressure was adjusted to the desired value for 1 min (3). The pressure was slowly released and then again adjusted to the desired level (4). Samples were incubated at room temperature for 10–20 min before measurements. After preincubation, the duration of measurements on the 20 samples of 1 holder was ≈10 min (total time of samples under pressure of 20–30 min). For measurements with control samples (ambient air atmosphere), an identical timing protocol was used.

PSII samples residing in the pressure cell were excited by a laser (Continuum Inlite-II, 532 nm, pulses of 5 ns and 50 mJ spaced by 700 ms); neighboring samples were shielded by a shutter. The X-ray fluorescence was detected by a large-area scintillation detector shielded against scattered X-rays by 10 μm of Cr foil and visible light by 2 μm of Al foil.

XANES spectra at the Mn K-edge were recorded within 1 s (irradiation time limited by a shutter, $\tau_{open} < 1$ ms) by using the rapid-scan mode of ID26 (27, 28). Samples were illuminated by 0–6 laser flashes; last flash ≈200 ms before the start of the monochromator scan. For a single XANES spectrum, ≈60 scans were averaged, each collected on a fresh sample. Spectra were normalized to an amplitude of 1.28 at 6,564 eV (22, 29).

In all time-resolved X-ray experiments with microsecond resolution, fluorescence transients were recorded for excitation at 6,552.5 eV. The samples were irradiated by the X-rays within a time interval of 5 ms before and 15 ms after each laser flash. For 1 transient, 500–1,000 measurements were collected, each on a fresh PSII sample, and averaged.

XANES spectra collected after application of 0–3 laser flashes were corrected for imperfect S-state advancement in the S-state cycle to yield the spectra of the pure S-states (36). For this deconvolution (and all simulations referred to in *Results*), we used a specific EXCEL spreadsheet that allowed for the joint simulation (least-squares curve-fitting) of the experimentally determined flash-number dependence of the K-edge energy (from XANES spectra) and the amplitude of the millisecond reduction phase of Mn in the O_2-evolving step (from exponential simulations of the time-resolved X-ray data).

ACKNOWLEDGMENTS. We thank M. Fünning for skillful preparation of PSII samples; D. Hund (mechanics workshop) for help in construction of the pressure cell; S. Krätzig from the workgroup of Prof. K. Gerwert (Bochum) for support in data collection; Dr. Friedhelm Lendzian (Technical University Berlin) for support in the EPR measurements; and the scientists at beamline ID26 of the European Synchrotron Radiation Facility, Drs. T.-C. Weng and P. Glatzel, for excellent technical support. This work was supported by Deutsche Forschungsgemeinschaft Grant Sonderforschungsbereich 498, the Bundesministerium für Bildung and Forschung Bio-H_2 Grant 035F0318C, the European Union SOLAR-H2 project, and UniCat Cluster of Excellence, Berlin. I.Z. was the recipient of an Alexander-von-Humboldt Foundation fellowship.

1. McEvoy JP, Brudvig GW (2006) Water-splitting chemistry of photosystem II. *Chem Rev* 106:4455–4483.
2. Zouni A, *et al*. (2001) Crystal structure of photosystem II from *Synechococcus elongatus* at 3.8 Å resolution. *Nature* 409:739–743.
3. Loll B, Kern J, Saenger W, Zouni A, Biesiadka J (2005) Towards complete cofactor arrangement in the 3.0 Å resolution structure of photosystem II. *Nature* 438:1040–1044.
4. Ferreira KN, Iverson TM, Maghlaoui K, Barber J, Iwata S (2004) Architecture of the photosynthetic oxygen-evolving center. *Science* 303:1831–1838.
5. Dau H, Haumann M (2008) The manganese complex of photosystem II in its reaction cycle: Basic framework and possible realization at the atomic level. *Coord Chem Rev* 252:273–295.
6. Beerling D (2007) *The Emerald Planet*: *How Plants Changed Earth's History* (Oxford Univ Press, New York).
7. Beerling DJ, Berner RA (2000) Impact of a Permo-Carboniferous high O_2 event on the terrestrial carbon cycle. *Proc Natl Acad Sci USA* 97:12428–12432.
8. Perchorowicz JT, Raynes DA, Jensen RG (1981) Light limitation of photosynthesis and activation of ribulose bisphosphate carboxylase in wheat seedlings. *Proc Natl Acad Sci USA* 78:2985–2989.
9. Sage RF, Cen YP, Li M (2002) The activation state of Rubisco directly limits photosynthesis at low CO_2 and low O_2 partial pressures. *Photosynth Res* 71:241–250.
10. Clausen J, Junge W (2004) Detection of an intermediate of photosynthetic water oxidation. *Nature* 430:480–483.

11. Clausen J, Junge W, Dau H, Haumann M (2005) Photosynthetic water oxidation at high O_2 backpressure monitored by delayed chlorophyll fluorescence. *Biochemistry* 44:12775–12779.
12. Raven JA, Larkum AW (2007) Are there ecological implications for the proposed energetic restrictions on photosynthetic oxygen evolution at high oxygen concentrations? *Photosynth Res* 94:31–42.
13. Yano J, *et al*. (2006) Where water is oxidized to dioxygen: Structure of the photosynthetic Mn_4Ca cluster. *Science* 314:821–825.
14. Dau H, Grundmeier A, Loja P, Haumann M (2008) On the structure of the manganese complex of photosystem II: Extended-range EXAFS data and specific atomic-resolution models for four S-states. *Philos Trans R Soc London Ser B* 363:1237–1244.
15. Kok B, Forbush B, McGloin M (1970) Cooperation of charges in photosynthetic O_2 evolution. I. A linear four-step mechanism. *Photochem Photobiol* 11:457–475.
16. Joliot P, Joliot A (1968) A polarographic method for detection of oxygen production and reduction of Hill reagent by isolated chloroplasts. *Biochim Biophys Acta* 153:625–634.
17. Dau H, Haumann M (2007) Eight steps preceding O—O bond formation in oxygenic photosynthesis: A basic reaction cycle of the photosystem II manganese complex. *Biochim Biophys Acta* 1767:472–483.
18. Grabolle M, Dau H (2007) Efficiency and role of loss processes in light-driven water oxidation by PSII. *Physiol Plant* 131:50–63.
19. Rappaport F, Guergova-Kuras M, Nixon PJ, Diner BA, Lavergne J (2002) Kinetics and pathways of charge recombination in photosystem II. *Biochemistry* 41:8518–8527.
20. Cser K, Vass I (2007) Radiative and nonradiative charge recombination pathways in photosystem II studied by thermoluminescence and chlorophyll fluorescence in the cyanobacterium *Synechocystis* 6803. *Biochim Biophys Acta* 1767:233–243.
21. de Wijn R, van Gorkom HJ (2002) The rate of charge recombination in photosystem II. *Biochim Biophys Acta* 1553:302–308.
22. Haumann M, *et al*. (2005) Photosynthetic O_2 formation tracked by time-resolved X-ray experiments. *Science* 310:1019–1021.
23. Dau H, Haumann M (2007) Time-resolved X-ray spectroscopy leads to an extension of the classical S-state cycle model of photosynthetic oxygen evolution. *Photosynth Res* 92:327–343.
24. Dau H, Haumann M (2006) Reaction cycle of photosynthetic water oxidation in plants and cyanobacteria. *Science* 312:1471–1472.
25. Junge W, Clausen J (2006) Photosynthetic oxygen production (letter). *Science* 312:1470–1471.
26. Penner-Hahn JE, Yocum CF (2006) Photosynthetic oxygen production (response). *Science* 312:1470–1471.
27. Meinke C, Sole VA, Pospisil P, Dau H (2000) Does the structure of the water-oxidizing photosystem II–manganese complex at room temperature differ from its low-temperature structure? A comparative X-ray absorption study. *Biochemistry* 39:7033–7040.
28. Haumann M, Grabolle M, Neisius T, Dau H (2002) The first room-temperature X-ray absorption spectra of higher oxidation states of the tetra-manganese complex of photosystem II. *FEBS Lett* 512:116–120.
29. Haumann M, Müller C, Liebisch P, Neisius T, Dau H (2005) A novel BioXAS technique with submillisecond time resolution to track oxidation state and structural changes at biological metal centers. *J Synchrotron Rad* 12:35–44.
30. Yachandra VK (1995) X-ray absorption spectroscopy and applications in structural biology. *Methods Enzymol* 246:638–678.
31. Penner-Hahn JE (1999) Structural characterization of the Mn site in the photosynthetic oxygen-evolving complex. In *Metal Sites in Proteins and Models: Redox Centres*, eds Hill HAO, Sadler PJ, Thomson AJ (Springer, Berlin), pp 1–36.
32. Dau H, Liebisch P, Haumann M (2003) X-ray absorption spectroscopy to analyze nuclear geometry and electronic structure of biological metal centers: Potential and questions examined with special focus on the tetra-nuclear manganese complex of oxygenic photosynthesis. *Anal Bioanal Chem* 376:562–583.
33. Grabolle M, Haumann M, Muller C, Liebisch P, Dau H (2006) Rapid loss of structural motifs in the manganese complex of oxygenic photosynthesis by X-ray irradiation at 10–300 K. *J Biol Chem* 281:4580–4588.
34. Dau H, Liebisch P, Haumann M (2004) The structure of the manganese complex of photosystem II in its dark-stable S_1-state: EXAFS results in relation to recent crystallographic data. *Phys Chem Chem Phys* 6:4781–4792.
35. Yano J, *et al*. (2005) X-ray damage to the Mn_4Ca complex in single crystals of photosystem II: A case study for metalloprotein crystallography. *Proc Natl Acad Sci USA* 102:12047–12052.
36. Haumann M, *et al*. (2005) Structural and oxidation state changes of the photosystem II manganese complex in four transitions of the water oxidation cycle ($S_0 \rightarrow S_1$, $S_1 \rightarrow S_2$, $S_2 \rightarrow S_3$, and $S_{3,4} \rightarrow S_0$) characterized by X-ray absorption spectroscopy at 20 K and room temperature. *Biochemistry* 44:1894–1908.
37. Dau H, Iuzzolino L, Dittmer J (2001) The tetra-manganese complex of photosystem II during its redox cycle: X-ray absorption results and mechanistic implications. *Biochim Biophys Acta* 1503:24–39.
38. Messinger J, *et al*. (2001) Absence of Mn-centered oxidation in the $S_2 \rightarrow S_3$ transition: Implications for the mechanism of photosynthetic water oxidation. *J Am Chem Soc* 123:7804–7820.
39. Krieger-Liszkay A (2005) Singlet oxygen production in photosynthesis. *J Exp Bot* 56:337–346.
40. Moller IM, Jensen PE, Hansson A (2007) Oxidative modifications to cellular components in plants. *Annu Rev Plant Biol* 58:459–481.
41. Pospisil P, Arato A, Krieger-Liszkay A, Rutherford AW (2004) Hydroxyl radical generation by photosystem II. *Biochemistry* 43:6783–6792.
42. Dismukes GC, Siderer Y (1981) Intermediates of a polynuclear manganese center involved in photosynthetic oxidation of water. *Proc Natl Acad Sci USA* 78:274–278.
43. Telfer A, Bishop SM, Phillips D, Barber J (1994) Isolated photosynthetic reaction center of photosystem II as a sensitizer for the formation of singlet oxygen: Detection and quantum yield determination using a chemical trapping technique. *J Biol Chem* 269:13244–13253.
44. Takizawa K, Cruz JA, Kanazawa A, Kramer DM (2007) The thylakoid proton motive force in vivo: Quantitative, noninvasive probes, energetics, and regulatory consequences of light-induced pmf. *Biochim Biophys Acta* 1767:1233–1244.
45. Schiller H, Dau H (2000) Preparation protocols for high-activity photosystem II membrane particles of green algae and higher plants, pH dependence of oxygen evolution, and comparison of the S_2-state multiline signal by X-band EPR spectroscopy. *J Photochem Photobiol B* 55:138–144. Vol. 105, No. 999